Infrared and TPD Studies of Nitrates Adsorbed on Tb_4O_7, La_2O_3, BaO, and MgO/γ-Al_2O_3

Yawu Chi and Steven S. C. Chuang*

Department of Chemical Engineering, The University of Akron, Akron, Ohio 44325-3906

Received: November 3, 1999; In Final Form: March 10, 2000

NO and O_2 coadsorption on γ-Al_2O_3-supported Tb_4O_7, La_2O_3, BaO, and MgO has been investigated by in situ infrared spectroscopy coupled with temperature-programmed decomposition and desorption. BaO/γ-Al_2O_3 and MgO/γ-Al_2O_3 possess a higher NO_x storage capability than Tb_4O_7/γ-Al_2O_3 and La_2O_3/γ-Al_2O_3. NO/O_2 coadsorbed on Tb_4O_7, La_2O_3, and BaO in the form of bridging bidentate, chelating bidentate, and monodentate nitrates, and on MgO in the form of bridging bidentate and monodentate nitrates via the reaction of adsorbed NO with adsorbed oxygen at 298 K. NO/O_2 coadsorbed as a chelating bidentate nitrate on Tb_4O_7 and La_2O_3, and as a distinctive bridging bidentate nitrate on BaO and MgO via the reaction of adsorbed NO with surface lattice oxygen at 523 K. These various forms of adsorbed nitrate differ in structure and reactivity from $Tb(NO_3)_3$, $La(NO_3)_3$, $Ba(NO_3)_2$, and $Mg(NO_3)_2$, the precursor used to prepare metal oxides for NO/O_2 coadsorption. Temperature-programmed desorption (TPD) of chelating bidentate nitrate on Tb_4O_7, La_2O_3, and BaO produced primarily NO and O_2, with maxima at 640 and 670 K, respectively. TPD of bridging bidentate nitrate and monodentate nitrate on Tb_4O_7, La_2O_3, and BaO produced NO and O_2 as major products and N_2 and N_2O as minor products, at 320−500 K. Decomposition of bridging bidentate on MgO produced NO as a major product and N_2O as a minor product at a peak temperature of 690 K. Peak temperatures for $Tb(NO_3)_3$, $La(NO_3)_3$, $Ba(NO_3)_2$, and $Mg(NO_3)_2$ decomposition occurred between those for bridging and chelating nitrates. The difference in stability between chelating and bridging bidentate nitrates on various metal oxides/γ-Al_2O_3 may provide a wide range of operating temperatures for NO_x storage.

1. Introduction

The control of NO emissions to meet increasingly stringent standards has been a major challenge for coal-fired power plants and automobile industries. No catalysts for NO removal in an oxidizing environment are found to have activities close to being practical. Catalytic approaches for the removal of NO include (1) the reaction of NO with CO over Rh−Pt and Pd-based catalysts in the catalytic converter,[1,2] (2) the reaction of NO and CO on metal oxides,[3,4] (3) the reaction of NO with hydrocarbons on Cu− and Co−ZSM-5[5−9] and alkali-MgO catalysts,[10−12] (4) the selective catalytic reduction (SCR) of NO with NH_3,[13,14] and (5) the direct decomposition of NO over Cu-,[15−19] Tb-,[20] and Ba-based[10−12,21−25] catalysts.

All these catalytic approaches involve (1) N−O bond dissociation of adsorbed NO or precursor containing NO to form adsorbed nitrogen and adsorbed oxygen; (2) combination of adsorbed nitrogen with itself or with other N-containing species to form gaseous nitrogen; (3) reaction of adsorbed oxygen with reducing agents such as CO, NH_3, and hydrocarbons; and/or (4) desorption of oxygen. Removal of adsorbed oxygen is required to complete the catalytic cycle of NO reduction. The direct decomposition of NO to nitrogen (N_2) and oxygen (O_2) appears to be an attractive approach; however, it suffers from poisoning by the presence of excess oxygen. No NO_x (i.e., NO and NO_2) removal catalysts for diesel/lean-burn engines are known to have activities close to being practical. Although the use of reducing agents effectively removes adsorbed oxygen, it complicates the NO removal process. In addition, it has limited the range of operating conditions, resulting in high capital and

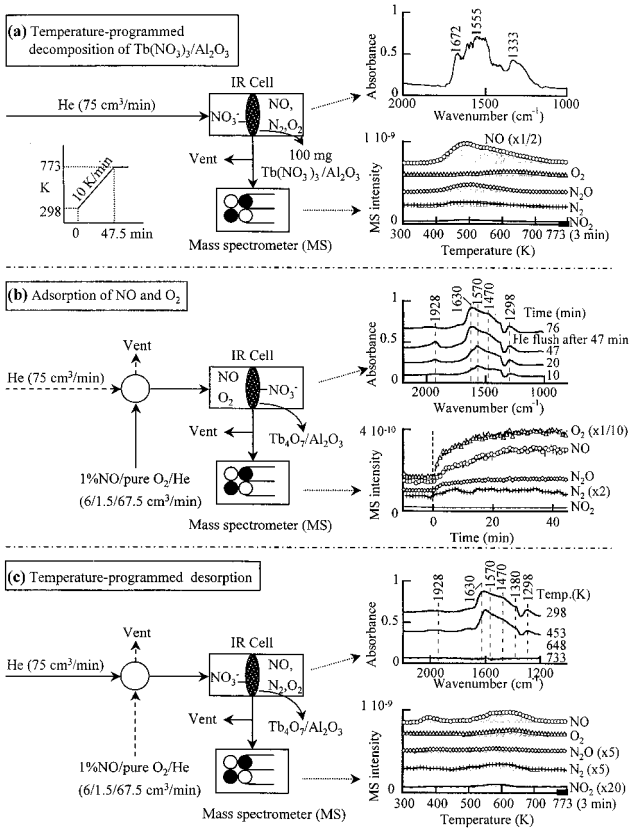

Figure 1. Experimental approach: (a) temperature-programmed decomposition of $Tb(NO_3)_3$/γ-Al_2O_3, (b) adsorption of NO and O_2 on Tb_4O_7/γ-Al_2O_3 at 298 K, and (c) temperature-programmed desorption of NO_x adsorbates on Tb_4O_7/γ-Al_2O_3 from 298 to 773 K.

* Author to whom all correspondence should be addressed. E-mail, schuang@uakron.edu, tel, (330) 972-6993; fax, (330) 972-5856.

10.1021/jp993894m CCC: $19.00
Published on Web 04/25/2000

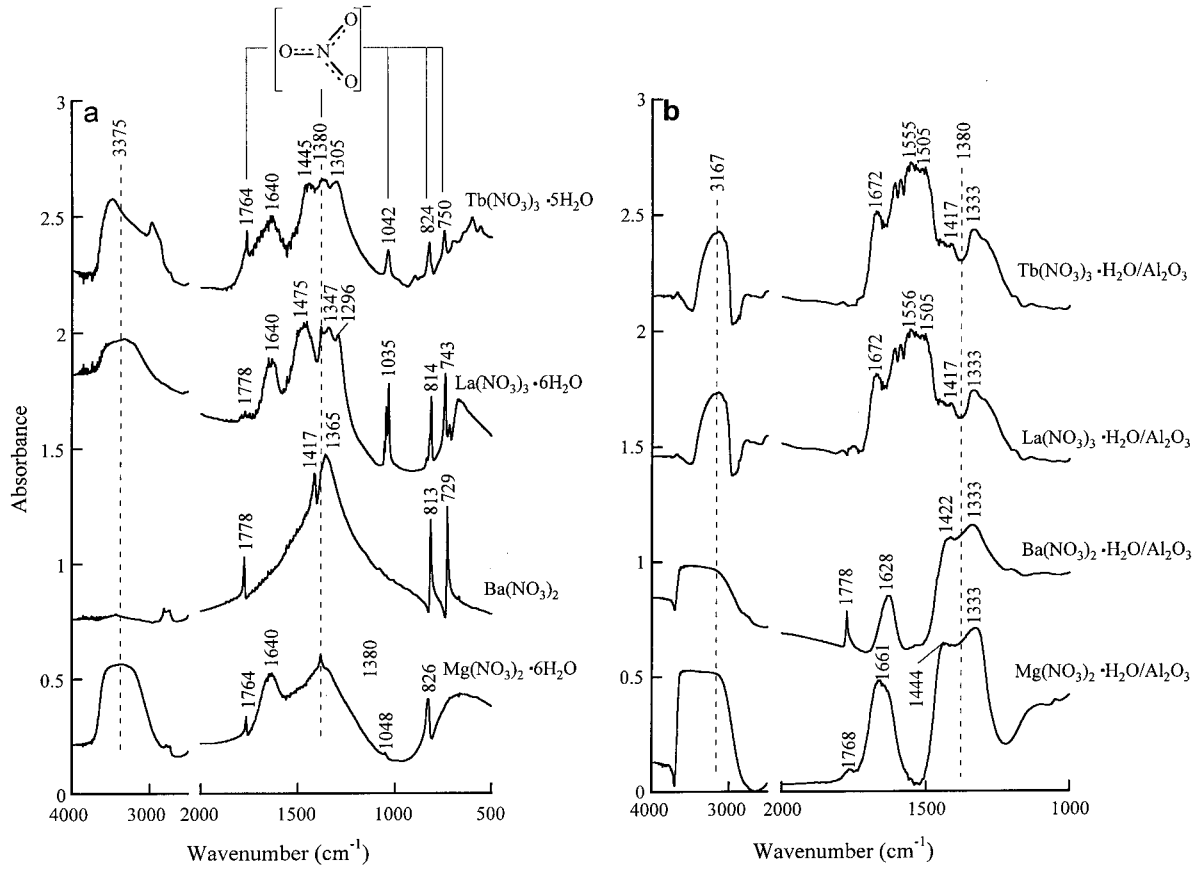

Figure 2. IR spectra of (a) original nitrates and (b) nitrates/γ-Al_2O_3 at 298 K.

TABLE 1: Loading of Nitrates and Metal Oxides on γ-Al_2O_3 and Particle Size

species	wt% in $M(NO_3)_n$	wt% in M_xO_y	wt% in M_xO_y needed for monolayer[a]	XRD analysis: crystal	XRD analysis: particle size (Å)
Tb	25.7	15.8 (Tb_4O_7)	12.4	Tb_4O_7	105
La	24.5	15.0 (La_2O_3)	5.4		
Ba	14.6	9.2 (BaO)	2.5	BaO	198
Mg	9.7	1.7 (MgO)	0.7		

[a] Estimated by packed monolayer model according to ref 47.

operating costs. The limiting operating temperature range is a result of the interaction of competing reactions: NO reduction and reductant oxidation. To avoid the direct oxidation of reductant, the concept of NO storage and reduction has been tested for removal of NO in an oxidizing environment. BaO−CuO,[21] Pt/Ba/Al_2O_3,[22] binary oxides (Ba−Cu, Mn−Y, and Mn−Zr),[23] Pt−Ba/washcoat,[24] and Cu-exchanged mordenite[25] have been tested for NO_x storage. A better understanding of NO/O_2 interaction with the NO_x storage medium is needed to move from the empirical material screening toward rational design.

The objective of this study is to investigate the adsorption of NO/O_2 on metal oxides and decomposition of their adsorbates. Tb,[20,26] La,[27−30] Ba,[10−12,24,31,32] and Mg[10−12,32−34] oxides are selected for this study due to their wide uses as promoters and storage mediums in automobile and lean-burn NO removal catalysts. This paper reports the results of an infrared study of (1) NO_x storage on metal oxides in an oxidizing environment and (2) desorption behavior of adsorbed NO_x on metal oxides.

2. Experimental Section

2.1. Preparation of γ-Al_2O_3-Supported Nitrates and IR Characterization. γ-Al_2O_3-supported $Tb(NO_3)_3$, $La(NO_3)_3$, $Ba(NO_3)_2$, and $Mg(NO_3)_2$ (Alfa Products) were prepared by incipient wetness impregnation of γ-Al_2O_3 (Alfa Products; surface area, 100 m^2/g; pore size, 0.01−0.02 μm) with a metal nitrate solution. The ratio of the volume of the solution to the weight of γ-Al_2O_3 was about 1 cm^3 to 2 g. The impregnated samples were dried overnight in air at room temperature. The loading of nitrate on γ-Al_2O_3 is listed in Table 1.

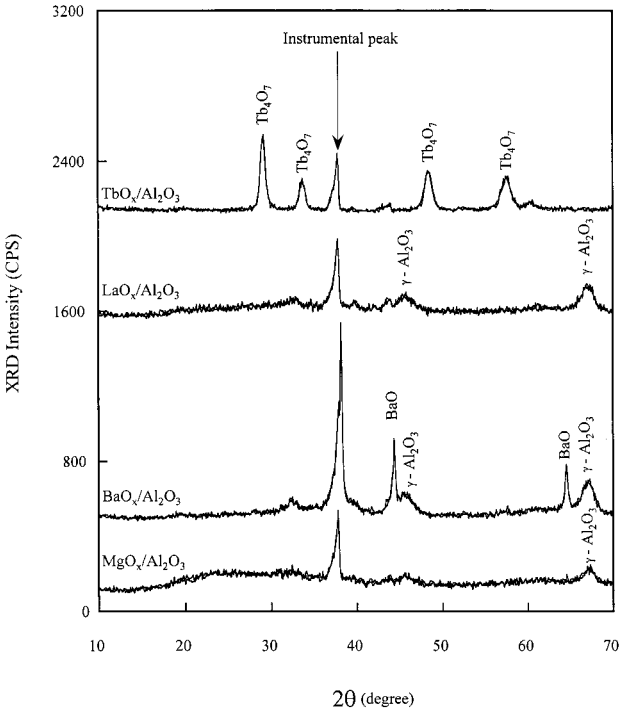

Figure 3. X-ray diffraction patterns of decomposed nitrates/γ-Al_2O_3.

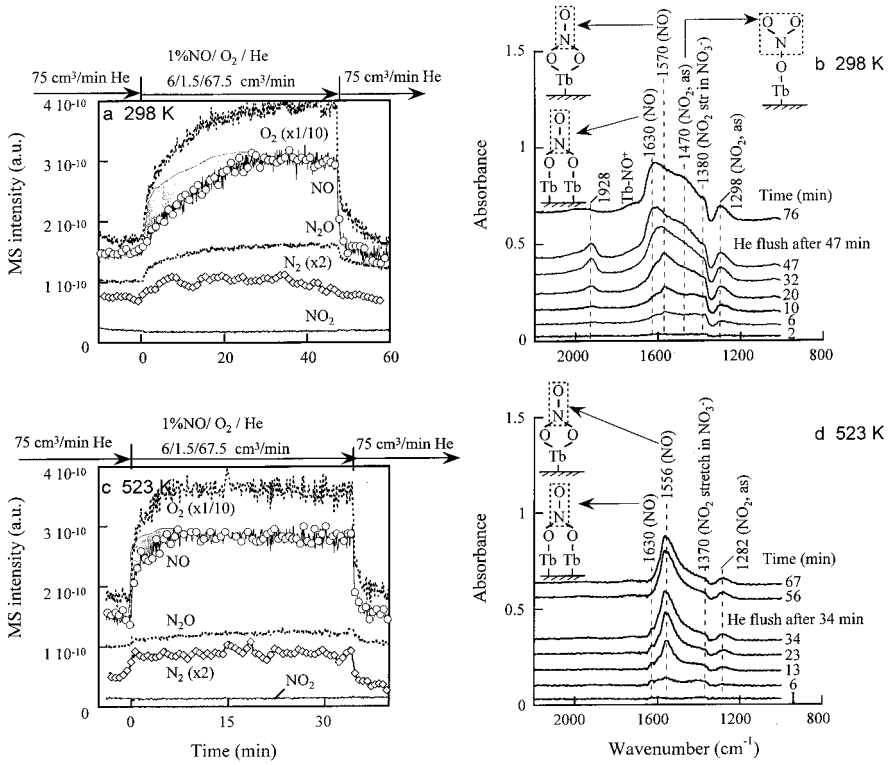

Figure 4. MS profiles and in situ IR spectra during 0.08% NO and 2% O_2 adsorption on $Tb_4O_7/\gamma\text{-}Al_2O_3$ at 298 (a, b) and 523 K (c, d).

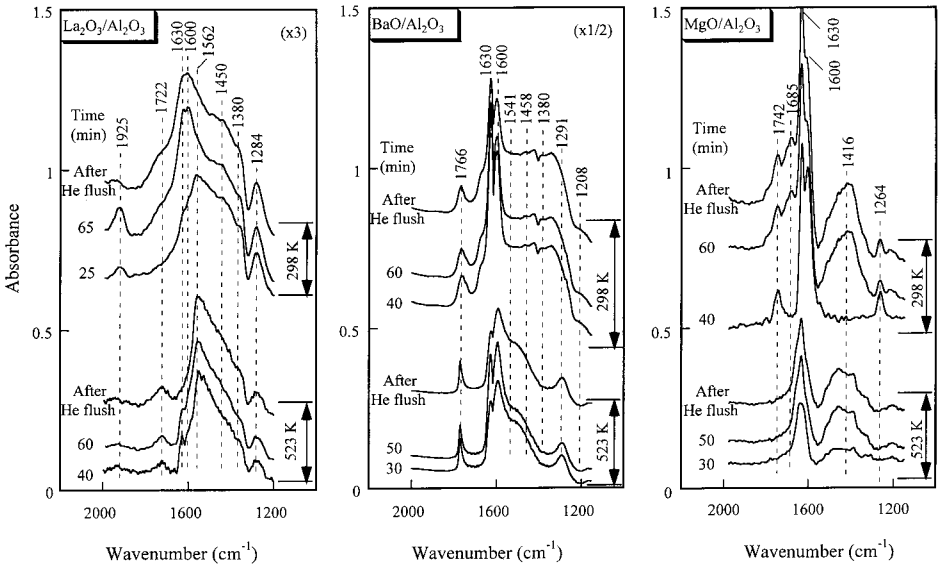

Figure 5. In situ IR spectra during 0.08% NO and 2% O_2 adsorption on $La_2O_3/\gamma\text{-}Al_2O_3$, $BaO/\gamma\text{-}Al_2O_3$, and $MgO/\gamma\text{-}Al_2O_3$ at 298 and 523 K.

The original metal nitrates and $\gamma\text{-}Al_2O_3$-supported nitrates (i.e., nitrates/$\gamma\text{-}Al_2O_3$) were mixed with KBr (Alfa Products, KBr spectrograde, ultrapure) at a weight sample/KBr ratio of 1:100 and pressed into self-supporting disks for infrared characterization at 298 K. The sample was mixed with KBr to obtain high resolution of nitrate bands. The IR spectra of $Tb(NO_3)_3{\cdot}6H_2O$, $La(NO_3)_3{\cdot}6H_2O$, $Ba(NO_3)_2$, and $Mg(NO_3)_2{\cdot}6H_2O$ were obtained by subtracting the KBr spectrum from each specific nitrate/KBr spectrum; the IR spectra of $Tb(NO_3)_3{\cdot}H_2O/\gamma\text{-}Al_2O_3$, $La(NO_3)_3{\cdot}H_2O/\gamma\text{-}Al_2O_3$, $Ba(NO_3)_2{\cdot}H_2O/\gamma\text{-}Al_2O_3$, and $Mg(NO_3)_2{\cdot}H_2O/\gamma\text{-}Al_2O_3$ were obtained by subtracting the $\gamma\text{-}Al_2O_3$/KBr spectrum from each specific nitrate/$\gamma\text{-}Al_2O_3$/KBr spectrum.

2.2. Adsorption and Decomposition/Desorption Studies. Figure 1 illustrates the experimental approach and sequence for study of each metal nitrate/$\gamma\text{-}Al_2O_3$. The experimental system consists of (1) the gas flow system with a 4-port switching valve and mass flow controllers for NO, O_2, and He; (2) the in situ IR reactor cell with self-supporting oxide disks; and (3) the analysis section with a Nicolet magna-IR 550 spectrometer for

TABLE 2: Amount of NO and O_2 Adsorption on Various Metal Oxides/$\gamma\text{-}Al_2O_3$ at 298 and 523 K

	at 298 K (μmol/g cat[a])		at 523 K (μmol/g cat[a])	
metal oxides	NO	O_2	NO	O_2
$Tb_4O_7/\gamma\text{-}Al_2O_3$	511	568	91	34
$La_2O_3/\gamma\text{-}Al_2O_3$	376	546	125	57
$BaO/\gamma\text{-}Al_2O_3$	724	1171	213	160
$MgO/\gamma\text{-}Al_2O_3$	377	32	226	<5

[a] Metal oxide/$\gamma\text{-}Al_2O_3$.

TABLE 3: IR Band Assignment of Adsorbates Produced from Flowing 0.08% NO and 2% O_2 over Various Metal Oxides/ γ-Al_2O_3 at 298 K and 523 K

	vibration mode and wavenumber (cm^{-1})[a]											
	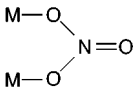 bridging bidentate		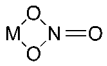 chelating bidentate		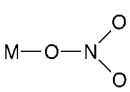 monodentate		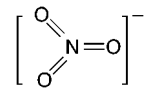 free NO_3^-					
metal oxides	N=O	$NO_{2,as}$	N=O	$NO_{2,as}$	$NO_{2,as}$	$NO_{2,sy}$	$NO_{2,as}$	M−(NO)$^+$	O−(NO)	O−(NO)$^-$	$N_2O_2^{2-}$	temp (K)
Tb_4O_7/Al_2O_3	1630	1298	1570	1298	1470		1380	1928				298
	1630	1282	1556	1282			1370					523
La_2O_3/Al_2O_3	1630	1284	1562	1284	1450		1380	1925		1722		298
	1600											
	1630	1284	1562	1284	1450		1375			1722		523
BaO/Al_2O_3	1630	1291	1541	1291	1458	1208	1380		1766	1672		298
	1600											
	1630	1291	1541	1291	1458				1766			523
	1600											
MgO/Al_2O_3	1630				1458	1207	1380			1678	1748[b]	298
	1600										1257	
	1630				1458	1207	1380					523

[a] Refs 16−34, 36−45. [b] Refs 34, 38.

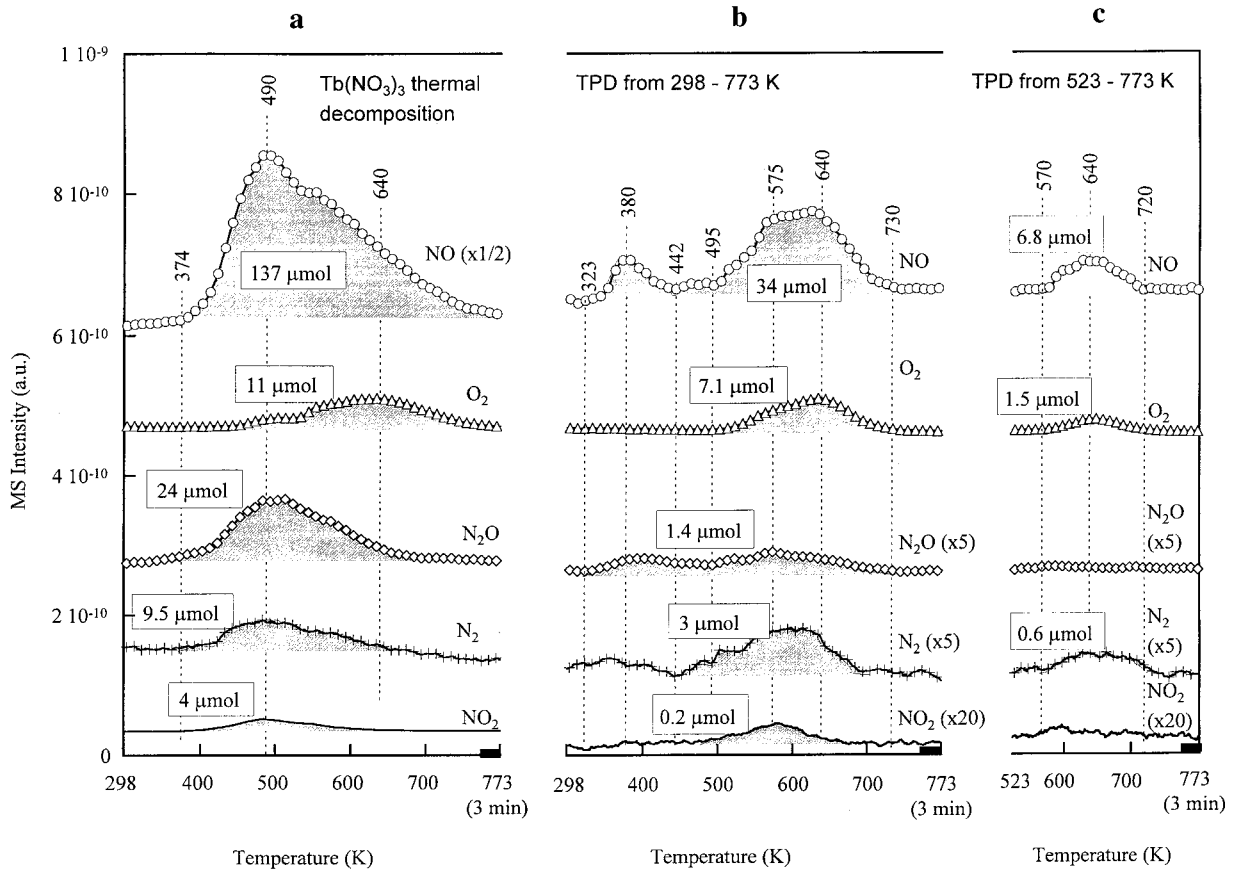

Figure 6. Normalized product MS profiles of (a) thermal decomposition of $Tb(NO_3)_3$ on γ-Al_2O_3, (b) TPD of adsorbates on Tb_4O_7/γ-Al_2O_3 from 298 to 773 K, and (c) TPD of adsorbates on Tb_4O_7/γ-Al_2O_3 from 523 to 773 K.

recording IR spectra of adsorbed species and a Balzers QMG 112 quadruple mass spectrometer (MS) for the analysis of reactant and product flows. The gaseous responses for He at $m/e = 4$, N_2 at $m/e = 28$, NO at $m/e = 30$, O_2 at $m/e = 32$, N_2O at $m/e = 44$, and NO_2 at $m/e = 46$ were monitored by the MS. Contribution of N_2O and NO_2 to fragments at $m/e = 30$ can be resolved from relative intensities of fragments and parent ions of the calibrated N_2O and NO_2 pulse responses.

To avoid complication from NO_x adsorption on KBr, 30 mg of fresh nitrate/γ-Al_2O_3 powder was pressed into a self-supporting disk without mixing with KBr and placed in the infrared beam path inside the infrared cell for temperature-programmed decomposition (TPDE), NO/O_2 adsorption, and temperature-programmed desorption (TPD) studies.[35] Additional nitrate/γ-Al_2O_3 disks with a total of 70 mg were broken into flakes and placed in the vicinity of the nitrate/γ-Al_2O_3 disk to increase the quantity of decomposed products in the reactor effluent, allowing accurate analysis of their compositions.

Metal nitrates/γ-Al_2O_3 underwent a series of studies: (1) TPDE studies from 298 to 773 K at a heating rate of 10 K/min in flowing He at 75 cm^3/min, (2) adsorption of NO/O_2 at 298

TABLE 4: Amount of Decomposed and Desorbed Product of γ-Al_2O_3-Supported Nitrates and Adsorbed Nitrates Produced from Flowing 0.08% NO/2% O_2 during TPDE/TPD

nitrates and metal oxides	NO_x storage ability[a] (%)	amount of decomposed and desorbed product (μmol)									TPDE/TPD
		NO	N_2	N_2O	NO_2	O_2	N_{total}	O_{total}	N/O	NO/O_2	
$Tb(NO_3)_3/Al_2O_3$		137	9.5	24	4	11	207	191	1.1	12.5	298−753 K (TPDE)
Tb_4O_7/Al_2O_3	57.8	34	3	1.4	0.2	7.1	43 (96%)[b]	50 (34%)[c]	0.9	4.8	298−753 K (TPD)
	10.8	6.8	0.6	trace	trace	1.5	8 (100%)	9.8 (70%)	0.8	4.5	523−753 K (TPD)
$La(NO_3)_3/Al_2O_3$		115	7	22	0.5	13	173.5	164	1.1	8.8	298−753 K (TPDE)
La_2O_3/Al_2O_3	42.3	28	1.3	0.5	0.3	8.2	31.9 (97%)	45.5 (35%)	0.7	3.4	298−753 K (TPD)
	13.7	9.8	0.3	none	trace	2.1	10.4 (95%)	14.0 (67%)	0.7	4.7	523−753 K (TPD)
$Ba(NO_3)_2/Al_2O_3$		83	8	6	1.3	10	112.3	111.6	1.0	8.3	298−753 K (TPDE)
BaO/Al_2O_3	118.2	62	1.3	0.6	0.4	20	66.2 (97%)	103.4 (40%)	0.6	3.1	298−753 K (TPD)
	33.2	18	0.2	trace	0.2	4.6	18.6 (93%)	27.6 (55%)	0.7	3.9	523−753 K (TPD)
$Mg(NO_3)_2/Al_2O_3$		57	0.7	4	1.2	none	67.6	63.4	1.1	*d*	298−753 K (TPDE)
MgO/Al_2O_3	87.8	31	none	0.8	0.8	none	33.4 (95%)	33.4 (81%)	1.0	*d*	298−753 K (TPD)
	54.5	19	none	0.7	0.3	none	20.7 (98%)	20.3 (97%)	1.0	*d*	523−753 K (TPD)

[a] Storage ability = total amount of N element of desorbed product during TPD (μmol/0.1 g cat)/total amount of metal cation in metal oxide/γ-Al_2O_3 (μmol/0.1 g cat) × 100%. [b] Ratio of desorbed N to adsorbed NO in parentheses. [c] Ratio of desorbed O to adsorbed O. [d] No O_2 was produced.

K over metal oxide/γ-Al_2O_3 produced from TPDE, (3) TPD study of NO/O_2 adsorbates from 298 to 773 K at a heating rate of 10 K/min in flowing He at 75 cm^3/min, (4) adsorption of NO/O_2 at 523 K over metal oxide/γ-Al_2O_3, and (5) TPD of NO/O_2 adsorbates from 523 to 773 K in He flow. Figure 1a−c shows the typical IR spectra of nitrates as well as MS profiles of gaseous species obtained during TPDE of $Tb(NO_3)_3$ on γ-Al_2O_3, NO/O_2 adsorption on Tb_4O_7/γ-Al_2O_3, and TPD studies. The metal oxides produced from TPDE of nitrates/γ-Al_2O_3 were characterized by X-ray diffraction (XRD) using a Philips Analytical, XRD B. V. diffractometer with Cu Kα radiation.

3. Results

3.1. IR Characterization of Metal Nitrates and Metal Nitrates/γ-Al_2O_3. Figure 2a,b compares the IR spectra of metal nitrates and metal nitrates/γ-Al_2O_3 at 298 K. All the nitrates used in this study exhibit typical nitrate bands at around 1380 cm^{-1} (NO_2 stretching, γ_3), 1037 cm^{-1} (NO stretching, γ_1), 814−826 cm^{-1} (out-of-plane bending, γ_2), 729−750 cm^{-1} (NO_2 bending, γ_4), and 1764−1778 cm^{-1} ($\gamma_1 + \gamma_4$).[36−45] The IR spectra of $Tb(NO_3)_3{\cdot}5H_2O$, $La(NO_3)_3{\cdot}6H_2O$, $Ba(NO_3)_2$, and $Mg(NO_3)_2{\cdot}6H_2O$ observed here agree well with those reported in the literature.[36,39] The bands at 3375 and 1640 cm^{-1} for $Tb(NO_3)_3{\cdot}5H_2O$, $La(NO_3)_3{\cdot}6H_2O$, and $Mg(NO_3)_2{\cdot}6H_2O$ can be attributed to H_2O. The absence of bands at around 3400 and 1630 cm^{-1} for anhydrous $Ba(NO_3)_2$ further confirms the H_2O assignment. $Tb(NO_3)_3{\cdot}5H_2O$ and $La(NO_3)_3{\cdot}6H_2O$, the lanthanide elements, exhibit the triplet in the 1290−1480 cm^{-1} region.

The γ-Al_2O_3 surface has a greater effect on Tb and La nitrates than on Ba and Mg nitrates. Figure 2b shows that the contour and wavenumber of IR bands for Ba and Mg nitrates are modified by the γ-Al_2O_3 support, probably because of the overlapping IR absorption of γ-Al_2O_3 and distortion of the nitrate structure induced by the γ-Al_2O_3 surface. In contrast, the triplet characteristics of free nitrate in the 1296−1475 cm^{-1} region decreased their intensities, and chelating nitrates at 1505−1580 cm^{-1} emerged on La and Tb nitrates on γ-Al_2O_3. It is interesting to observe that the nitrates of the elements in the same group exhibit a similar vibration frequency, indicating the similarity in their structures.

3.2. XRD Determination. Figure 3 shows the XRD patterns of metal oxides/γ-Al_2O_3 produced from the thermal decomposition of nitrates/γ-Al_2O_3. Tb and Ba oxides gave distinct X-ray diffraction patterns for Tb_4O_7 and BaO, whose crystallite sizes were determined to be 117.2 and 220.8 Å, respectively, by the Scherrer equation.[46] The absence of XRD patterns for La and Mg oxides suggests that these oxides were highly dispersed on γ-Al_2O_3 with a crystallite size less than 30 Å. Those oxides produced from nitrate decomposition were denoted as Tb_4O_7/γ-Al_2O_3, La_2O_3/γ-Al_2O_3, BaO/γ-Al_2O_3, and MgO/γ-Al_2O_3 in this study because they are the most abundant forms of oxides on γ-Al_2O_3, as evidenced by XRD. Table 1 lists the loading of metal nitrates and metal oxides, and the weight percentage needed for achieving a monolayer dispersion[47] of each metal oxide on γ-Al_2O_3. Loading of La_2O_3, BaO, and MgO is sufficiently high to achieve more than two layers of oxides on the surface of γ-Al_2O_3. XRD results indicate that Tb_4O_7 and

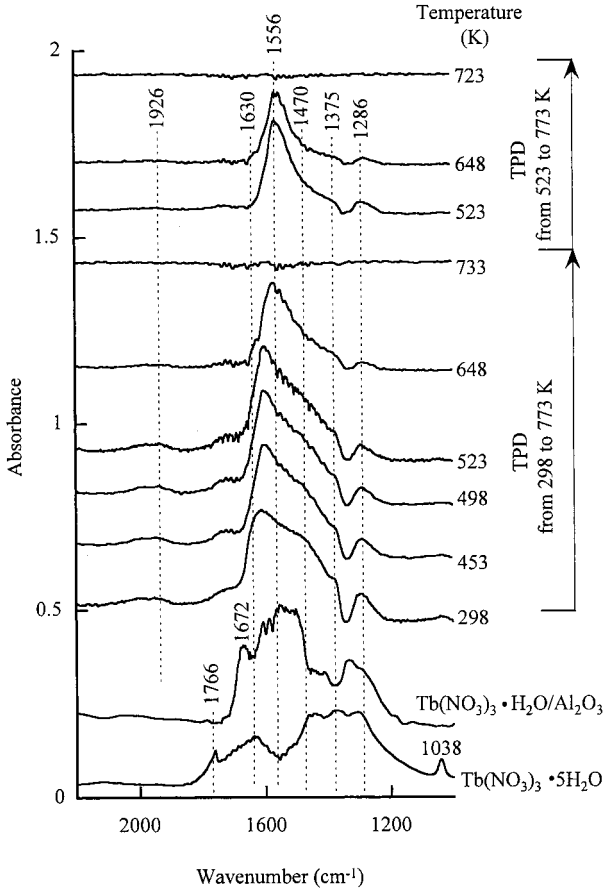

Figure 7. In situ IR spectra during TPD of adsorbates on Tb_4O_7/γ-Al_2O_3 from 298/523 to 773 K as well as IR spectra of $Tb(NO_3)_3{\cdot}H_2O/\gamma$-$Al_2O_3$ and $Tb(NO_3)_3{\cdot}6H_2O$ at 298 K.

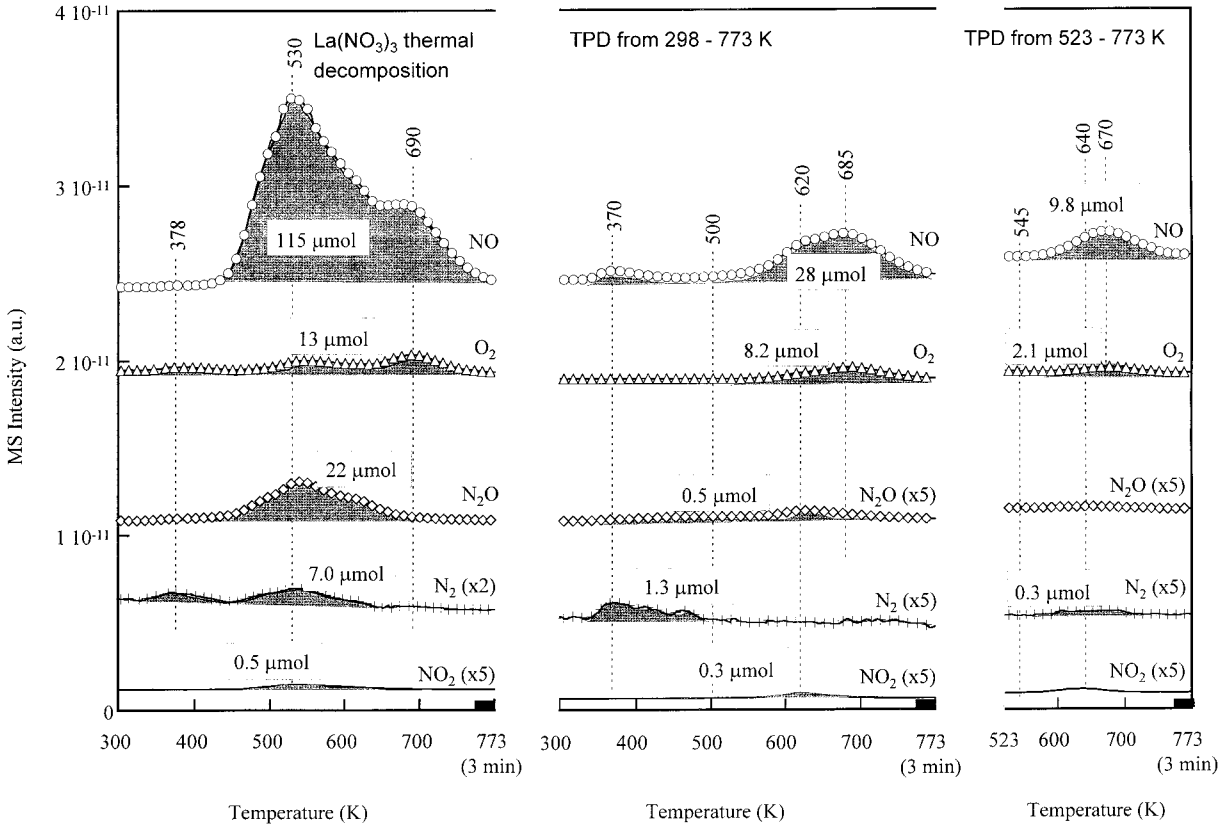

Figure 8. Normalized product MS profiles of (a) thermal decomposition of $La(NO_3)_3$ on γ-Al_2O_3, (b) TPD of adsorbates on La_2O_3/γ-Al_2O_3 from 298 to 773 K, and (c) TPD of adsorbates on La_2O_3/γ-Al_2O_3 from 523 to 773 K.

BaO aggregated on the surface as particles. The absence of XRD patterns for aluminate-containing mixed oxides suggests the lack of extensive interaction/reaction between the supported oxides and γ-Al_2O_3. The possibility of the formation of La, Mg, and Ba aluminate can be ruled out because their formation occurred at temperatures above 1000 K.[48−51] It should be noted that lanthanum is the structural promoter most commonly used to stabilize Al_2O_3 against thermal sintering.[51] Improvement of hydrothermal stability of Al_2O_3 has also been observed with MgO and BaO promoters.

3.3. Adsorption of NO and O_2 on Metal Oxides/γ-Al_2O_3. Figure 4 shows the MS profiles of the reactor effluent and in situ IR spectra of adsorbates produced from flowing 0.08% NO/2% O_2 in He over Tb_4O_7/γ-Al_2O_3 at 298 K (Figure 4a,b) and 523 K (Figure 4c,d), respectively. NO/O_2 flow was introduced into the reactor by a step-switch from He flow to NO/O_2/He flow. The use of a well-defined step switch allows observation of adsorbate evolution and accurate determination of the amount of NO adsorbed. The amount of NO adsorbed at 298 and 523 K corresponds to the shaded area in Figure 4a,c, respectively. Table 2 lists the amount of NO adsorbed at 298 and 523 K on Tb_4O_7/γ-Al_2O_3 and other oxides/γ-Al_2O_3 used in this study. Exposure of Tb_4O_7/γ-Al_2O_3 to NO/O_2/He flow at 298 K produced (1) N_2O and N_2, as shown by the increase in N_2O and N_2 MS profiles in Figure 4a, and (2) bridging bidentate nitrate ($^{Tb-O}_{Tb-O}$ > N−O) at 1630 cm^{-1} and chelating bidentate nitrate ($Tb\langle^{O}_{O}\rangle N-O$) at 1570 cm^{-1}, with their asymmetric NO_2 stretching overlap at around 1298 cm^{-1}; monodentate nitrate ($Tb-O-N < ^{O}_{O}$) at 1470 cm^{-1}, NO_3^- at 1380 cm^{-1},[44,45] and $Tb-NO^+$ at 1928 cm^{-1}. It should be noted that the broad IR band in the region of 1380−1630 cm^{-1}, which is the result of multiple overlapping bands, could not be unambiguously determined due to the ill-defined oxide surface. Band assignment here follows the reported classical works,[44,45] previous literature,[16−34,36−43] and IR spectra of nitrates and nitrates/γ-Al_2O_3 in Figure 2. The low intensity of the bands in the 1300−1450 cm^{-1} region for NO_3^- indicates that $Tb(NO_3)_3$ was not reconstructed on Tb_4O_7/γ-Al_2O_3. Flowing NO/O_2 at 523 K produced (1) more N_2 but less N_2O than that at 298 K and (2) a dominant $Tb\langle^{O}_{O}\rangle N-O$ at 1556 and 1282 cm^{-1}. NO approached steady state faster at 523 K than at 298 K. The lack of $Tb-NO^+$ at 523 K may be due to the oxidization of adsorbed NO^+ to $Tb\langle^{O}_{O}\rangle N-O$.

Figure 5 compares the in situ IR spectra of adsorbates produced from flowing NO/O_2 over La_2O_3/γ-Al_2O_3, BaO/γ-Al_2O_3, and MgO/γ-Al_2O_3 at 298 and 523 K. Band assignment of these various adsorbates is summarized in Table 3. In general, bridging bidentate nitrate ($^{M-O}_{M-O}$ > N−O) exhibits a NO vibration band at 1600−1650 cm^{-1} and a weak NO_2 asymmetric vibration band at 1170−1225 cm^{-1}. Chelating bidentate nitrate ($M\langle^{O}_{O}\rangle$> N−O) gives a NO vibration band at 1500−1565 cm^{-1} and a weak NO_2 asymmetric vibration band at 1260−1300 cm^{-1}. Monodentate nitrate ($M-O-N < ^{O}_{O}$) shows a NO_2 asymmetric vibration band at 1480−1530 cm^{-1} and a weak NO_2 symmetric vibration band at 1250−1290 cm^{-1}. Nitrate (NO_3^-) displays a NO_2 stretching band at around 1380 cm^{-1}.[44,45] IR spectra of adsorbates produced from La oxide resemble those on Tb oxide despite the significant difference in their crystallite size and in the stoichiometry of Tb_4O_7 and La_2O_3 (i.e., the possible form of La oxide). Adsorbed nitrates on BaO and MgO show distinct bridging bidentate nitrate bands at 1630 cm^{-1} and $N_2O_2^{2-}$ on MgO at 1748 and 1257 cm^{-1}.[34,52] The formation of bridging bidentate nitrate on MgO is significantly faster than that of monodentate nitrate at 298 K. The IR intensity corre-

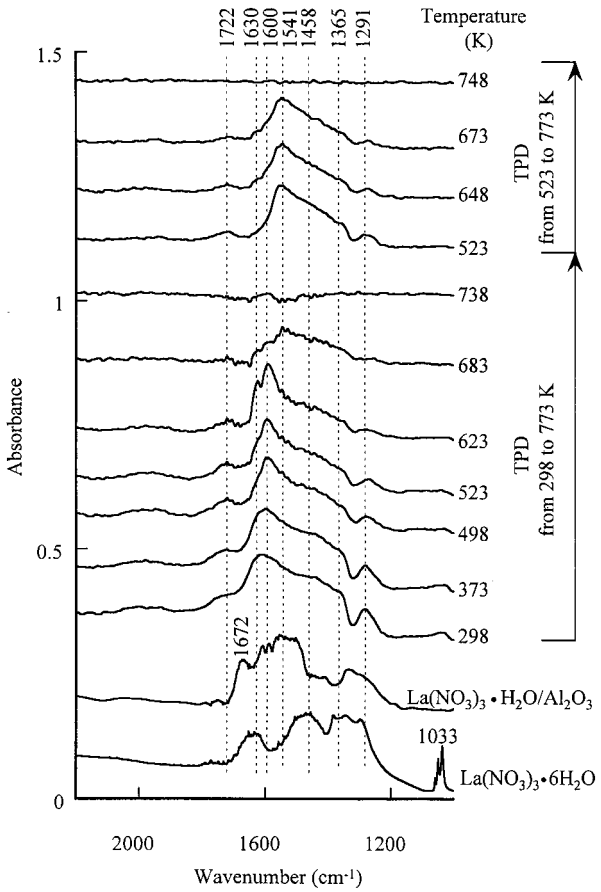

Figure 9. In situ IR spectra during TPD of adsorbates on La_2O_3/γ-Al_2O_3 from 298/523 to 773 K as well as IR spectra of $La(NO_3)_3{\cdot}H_2O/\gamma$-$Al_2O_3$ and $La(NO_3)_3{\cdot}6H_2O$ at 298 K.

sponds to the concentration of adsorbates, also reflecting the number of specific adsorption sites for these adsorbates. However, a lack of extinction coefficients for these various forms of adsorbed NO_x species does not allow use of these adsorbate intensities to determine the number of adsorption sites.

3.4. TPDE and TPD Studies. Figure 6 compares the normalized product MS profiles during TPDE of $Tb(NO_3)_3$ on γ-Al_2O_3 (Figure 6a) to those during TPD of adsorbates on Tb_4O_7/γ-Al_2O_3 from 298 to 773 K (Figure 6b) and from 523 to 773 K (Figure 6c) in He flow. These adsorbates were produced from NO/O_2 adsorption at 298 and 523 K, respectively. $Tb(NO_3)_3$ began to decompose at 374 K, releasing NO, O_2, N_2O, N_2, and NO_2 with a total amount of 185.5 μmol, a N/O ratio of 1.1, and a NO/O_2 ratio of 12.5. The MS intensity profiles were normalized with the calibration factors of each species so that the shaded area under the MS profiles corresponds to the product amount. Table 4 lists the amount of products produced from TPDE of γ-Al_2O_3-supported nitrates and TPD of adsorbates on metal oxides. Because NO is the dominant product, the ratio of N to O for all the products is near 1, indicating that decomposition of nitrates leaves oxygen on the metal oxide surface.

Figure 7 shows the in situ IR spectra of adsorbed NO_x on Tb_4O_7/γ-Al_2O_3 taken during TPD from 298 to 773 K and from 523 to 773 K, as well as the IR spectra of $Tb(NO_3)_3{\cdot}5H_2O$ and $Tb(NO_3)_3{\cdot}H_2O/\gamma$-$Al_2O_3$. The IR bands below 1200 cm^{-1} for nitrates/γ-Al_2O_3 and adsorbed NO_x on metal oxides/γ-Al_2O_3 were blocked by the γ-Al_2O_3 support and CaF_2 windows. Decrease in IR intensity with increasing temperature is indicative of desorption/decomposition of adsorbates on Tb_4O_7/γ-Al_2O_3, suggesting that these adsorbates are responsible for the formation of NO, O_2, N_2O, N_2, and NO_2. The decrease in chelating bidentate nitrate, which was produced from NO/O_2 adsorption at 523 K in Figure 7, corresponds to a symmetric NO, O_2, and N_2 desorption profile with the N/O molar ratio of 0.8 centered at 640 K in Figure 6c, indicating the conversion of this nitrate to NO and O_2. The small amount of desorbed O_2 suggests that the chelating bidentate nitrate decomposed primarily to NO, leaving oxygen on the metal oxide surface. The NO desorption centered at 640 K in Figure 6c has also been observed for NO TPD from 298 to 773 K in Figure 6b. The NO desorption at 640 K in Figure 6b is indeed a result of decomposition of chelating bidentate nitrate at 1556 cm^{-1} as shown in Figure 7. The most interesting observations in Figures 6 and 7 are that (1) N_2 was produced as a minor product and (2) the amount of NO, O_2, N_2, and N_2O desorbed from nitrates adsorbed on Tb_4O_7/γ-Al_2O_3 is significantly less than the decomposition of the original nitrate. It appears that metal oxide produced from $Tb(NO_3)_3$ decomposition has agglomerated and decreased the number of surface metal cations available for adsorption. Furthermore, each Tb in $Tb(NO_3)_3$ accommodates three $(NO_3)^-$, while each Tb in bridging and chelating bidentate nitrates and monodentate nitrate can accommodate only one $(NO_3)^-$.

Figures 8 and 9 show the product MS profiles and IR spectra during TPDE of $La(NO_3)_3{\cdot}H_2O/\gamma$-$Al_2O_3$ and subsequent TPD studies on La_2O_3/γ-Al_2O_3. TPDE of $La(NO_3)_3{\cdot}H_2O/\gamma$-$Al_2O_3$ exhibited IR and MS patterns similar to those of $Tb(NO_3)_3{\cdot}H_2O/\gamma$-$Al_2O_3$. N_2 formation on La_2O_3/Al_2O_3 is less than that on Tb_4O_7/γ-Al_2O_3.

Figures 10 and 11 show the MS profiles and IR spectra during TPDE of $Ba(NO_3)_2{\cdot}H_2O/\gamma$-$Al_2O_3$ and subsequent TPD studies on BaO/γ-Al_2O_3. TPDE of $Ba(NO_3)_2$ on γ-Al_2O_3 exhibited different MS profile patterns from those for $Tb(NO_3)_3$ and $La(NO_3)_3$, with only one O_2 desorption peak at 725 K.

Although $Ba(NO_3)_2/\gamma$-Al_2O_3 and $Mg(NO_3)_2/\gamma$-Al_2O_3 exhibit similar IR spectra, as shown in Figure 2, their TPDE and TPD/IR profiles show dramatic differences, as shown in Figures 10–13. The major difference is the absence of O_2 during the TPDE of $Mg(NO_3)_2$ and the TPD of NO/O_2 adsorbates on MgO/γ-Al_2O_3. The latter is due to the lack of O_2 adsorption during NO/O_2 adsorption at 298 and 523 K. In addition, bridging bidentate nitrate is centered at 1630 cm^{-1} on MgO and at 1600 cm^{-1} on BaO at 523 K. The former decomposed to NO and N_2O while the latter decomposed to NO and O_2, reflecting their differences in structure and reactivity.

4. Discussion

4.1. Formation of Adsorbed Nitrate. Adsorption of NO and O_2 on Tb_4O_7, La_2O_3, BaO, and MgO proceeds through a different pathway and pattern from that on noble metals. NO adsorbs on the reduced noble metal through the N atom in the form of M^0–NO (where M^0 is the reduced metal site).[53–56] NO stands either perpendicularly or titled to the surface, depending on the nature of the surface sites. Coadsorption of NO and O_2 usually leads to the formation of M^+–NO where M^+ is formed by oxidation of M^0. M^+–NO has often been denoted as $M{-}NO^+$.[53–56] Interestingly, this type of $M{-}NO^+$ has been observed on Tb_4O_7 and La_2O_3. The presence of $M{-}NO^+$ on Tb_4O_7 and La_2O_3 could be due to the nonstoichiometric nature of Tb and La oxides where their cations are exposed for direct NO adsorption.

Because of the ill-defined states of the surfaces of these oxides, the elementary steps involved in the formation of nitrates from NO/O_2 adsorption are significantly more difficult to elucidate than those on noble metals. NO/O_2 coadsorption on

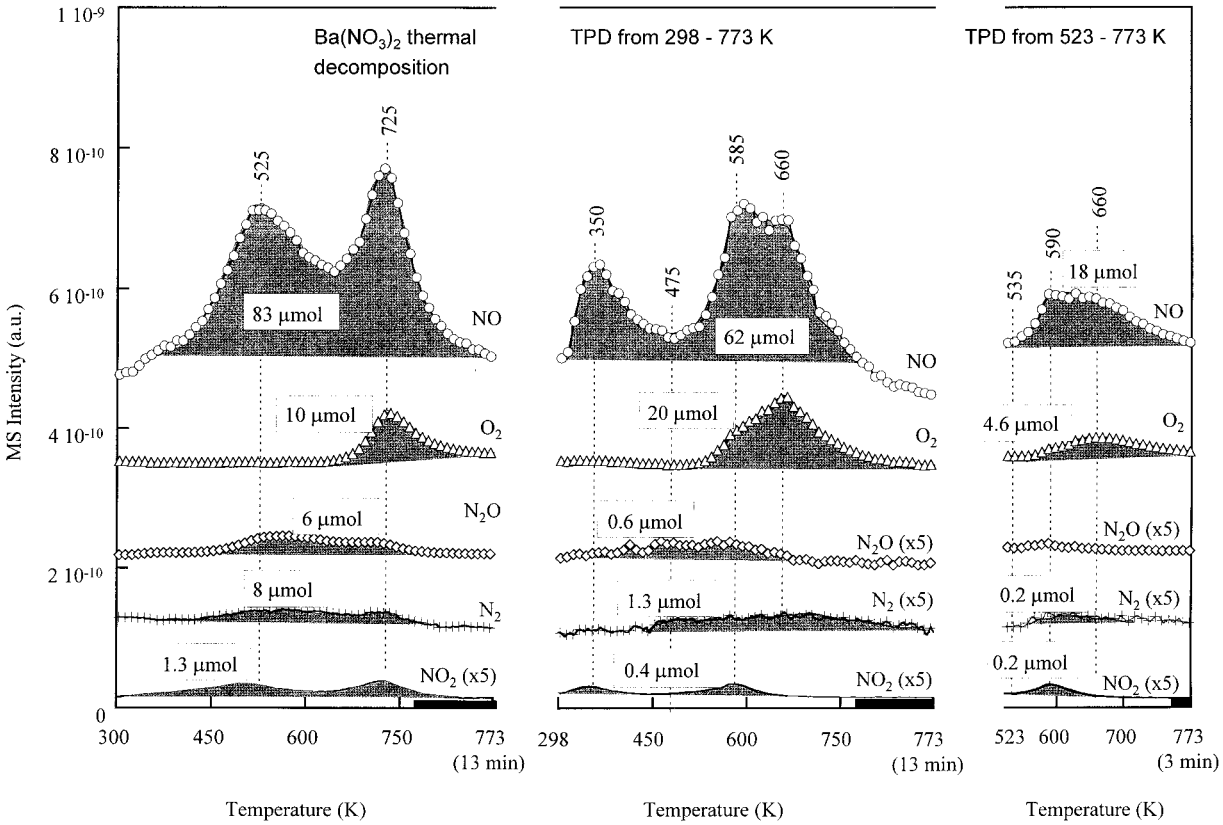

Figure 10. Normalized product MS profiles of (a) thermal decomposition of $Ba(NO_3)_2$ on γ-Al_2O_3, (b) TPD of adsorbates on BaO/γ-Al_2O_3 from 298 to 773 K, and (c) TPD of adsorbates on BaO/Al_2O_3 from 523 to 773 K.

these oxides produced three types of nitrates: bridging bidentate, chelating bidentate, and monodentate nitrates. In addition, trace amounts of N_2 and N_2O were produced, indicating the occurrence of N−O bond dissociation and N−N bond formation. These two steps occurred to a very limited extent on the oxide surface, as evidenced by low product formation rates. N−O bond dissociation is expected to occur on the unsaturated coordination sites where there are deficiencies in oxygen coordination.[57−60] N−N bond formation, a facile process, could be immediately followed by N−O dissociation. Coadsorption of NO and O_2 allows O_2 to compete for unsaturated coordination sites, further decreasing the N_2 and N_2O formation.

O_2 may adsorb on the oxide surface according to the following sequence:[61−63]

$$O_2(g) \leftrightarrow O_2(ads) \overset{+e}{\leftrightarrow} O_2^{-}\ (ads) \overset{+e}{\leftrightarrow} O_2^{2-}\ (ads) \leftrightarrow 2O^{-}\ (ads) \overset{+2e}{\leftrightarrow} 2O^{2-}\ (lattice)$$

Electron spin resonance (ESR) studies of adsorbed oxygen on TiO_2, ZnO, Fe_2O_3, MgO, and NiO provide evidence to support O_2^- formation.[61,62,64−67] This type of oxygen is stable at 298 K. Increasing temperature causes transformation of O_2^- to O^{2-} (i.e., lattice oxygen).[62,64,67−69] Thus, which types of adsorbed oxygen predominate may depend on the type and state of the surface and temperature. The metal cation may serve as an electron donor, allowing electron transfer to oxygen and increasing the oxidation state of the cation.[68] The nonstoichiometric metal oxides, such as Tb_4O_7, and those oxides with redox properties may allow oxidation of their cations.

Formation of bridging bidentate nitrate, chelating bidentate nitrate, and monodentate nitrate from NO and O_2 adsorption on Tb_4O_7, La_2O_3, and BaO may involve different forms of adsorbed oxygen which serve as a Lewis base site. The overall reaction may be written as:

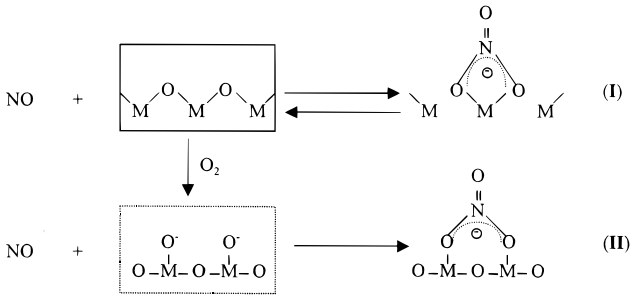

The formation of chelating bidentate nitrate has been observed on NO adsorption on Tb_4O_7.[70] Results in Figure 4 show that coadsorption of NO and O_2 on Tb_4O_7 produced both bridging and chelating bidentate nitrates at 298 K and formed only chelating bidentate nitrates at 523 K. Similar observations have been reported on oxidized chromia.[71] The N−O single bond in chelating bidentate nitrate appears to come from the lattice oxygen of the oxide, whereas the oxygen in bridging bidentate nitrate could result from adsorbed oxygen. The adsorbed oxygen may be in the form of O^- which locates in a configuration favoring the bridging bidentate nitrate formation. This proposed scheme explains the formation of a dominant chelating bidentate band at 523 K and the formation of a bridging bidentate nitrate at 298 K, where significantly more O_2 is adsorbed than at 523 K as shown in Table 2. The absence of adsorbed nitro species and NO_2 in the product stream indicates either the lack of surface sites available for the NO + O^- reaction or the rapid conversion of nitro/NO_2 species to nitrates.

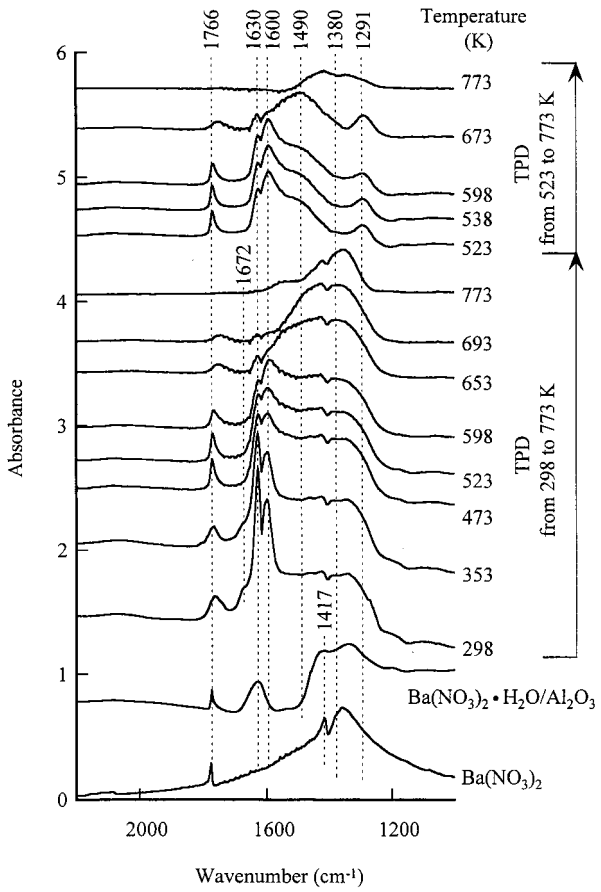

Figure 11. In situ IR spectra during TPD of adsorbates on BaO/γ-Al_2O_3 from 298/523 to 773 K as well as IR spectra of $Ba(NO_3)_2{\cdot}H_2O$/γ-Al_2O_3 and $Ba(NO_3)_2$ at 298 K.

Pretransition metal oxides such as MgO are very inert and can neither be oxidized nor reduced easily.[68,72] It is indeed not surprising to observe the low O_2 adsorption capability on MgO. Although MgO lacks O_2 adsorption capability, gaseous O_2 can exchange with O on the solid surface.[59] The bridging bidentate nitrate could be formed from NO adsorption coupled with oxygen exchange.

BaO and MgO, the alkali earth elements, show distinct differences in their TPDE and TPD/IR profiles. BaO is known for its exceptional capability for NO_x storage.[24,31] Results in Figure 5 show that NO and O_2 coadsorb on BaO as bridging bidentate, chelating bidentate, and monodentate nitrates at 298 and 523 K. Lunsford and co-workers[10−12] reported that flowing NO alone over defect-rich BaO/MgO produced nitrates, nitrites, and Ba-nitro complexes; exposure of nitrite/nitro species to oxygen led to the formation of NO_3^-; exposure of BaO_2 to NO produced nitro and NO_3^-. Our recent study[73] on CuO/γ-Al_2O_3 showed that the successive oxidation of adsorbed nitrite and nitro species produced various forms of nitrate during NO/O_2 coadsorption. All of these studies reveal that nitrate is the final form of the products on the oxide surface regardless of sequence of NO/O_2 adsorption or coadsorption. Excellent O_2 adsorption capability can be attributed to (1) its unsaturation sites and (2) reaction as $BaO + 1/2O_2\ (g) \Leftrightarrow BaO_2$.[74] BaO_2 has been produced during NO decomposition on BaO/MgO.[10−12]

4.2. Nitrate Decomposition. TPDE/TPD of nitrates in Figures 7−13 shows that NO and O_2 are the major decomposition products. TPD from 523 to 773 K for chelating bidentate nitrate (produced from NO/O_2 adsorption at 523 K) on Tb_4O_7, La_2O_3, and BaO gave primarily NO and O_2 product at a ratio of NO/O_2 of 4.5−3.9, suggesting that reaction I is essentially reversible. About 80% of oxygen in chelating bidentate nitrate on Tb_4O_7 and La_2O_3 returned to the oxygen lattice form on the oxides.

Chelating bidentate nitrate appears to be the most stable form of nitrate on Tb_4O_7, La_2O_3, and BaO. Bridging bidentate nitrate and other forms of nitrates which were produced from NO/O_2 adsorption decomposed at temperatures lower than chelating bidentate nitrate, producing N_2O, N_2, NO_2, NO, and O_2 on Tb_4O_7, La_2O_3, and BaO. Bridging bidentate nitrate, a major nitrate, on MgO also produced N_2O, N_2, and NO_2. Formation of a small amount of N_2 and N_2O during TPDE/TPD of nitrates suggests the occurrence of N−O bond dissociation and N−N bond formation between these nitrate species.

Consistency in the TPD peak temperatures of NO and O_2 for the NO/O_2 adsorbates at 298 and 523 K suggests that the nature of adsorption sites for the nitrate formation was not affected by the heating cycle. Repeated NO/O_2 adsorption and TPDE studies on Pt−Tb/γ-Al_2O_3[75] show that the heating cycle did not affect adsorption and desorption characteristics of adsorbed nitrates. Further study is needed to determine the effect of the heating cycle on the performance of these supported oxides. It should be noted that the amount of O_2 desorbed (measured by TPD profile) is less than that of adsorbed (measured by the step response profile), except for MgO/γ-Al_2O_3, as shown in Table 4. This discrepancy may be attributed to the readsorption of oxygen and the reaction of O_2 with other species in the mass spectrometer chamber. Underestimation of O_2 was also observed in the TPDE of nitrate/γ-Al_2O_3.

TPDE of the $Tb(NO_3)_3$, $La(NO_3)_3$, and $Ba(NO_3)_2$ produced more N_2O than TPD of the nitrates produced from NO/O_2 adsorption, as shown in Table 4. This observation indicates that these metal nitrates on γ-Al_2O_3 in the forms of mixed nitrates (i.e., NO_3^-, bridging and chelating bidentate nitrates) produced significantly more N_2O than other forms of nitrates. The infrared and mass spectrometer results reported here do not allow elucidation of the elementary steps involved in the N_2 and N_2O formation. Formation of N_2 on Tb_4O_7 could be attributed to its nonstoichiometric nature and redox property. The formation of N_2 from nitrate decomposition suggests the possibility of NO decomposition in an oxidizing environment through nitrates, as follows:

$$NO + O_2 \Leftrightarrow \text{nitrate} \Rightarrow N_2 + N_2O + O_2$$

Formation of N_2, O_2, and NO_2 has been observed during the decomposition of calcium nitrates.[76] However, the amount of N_2 produced remained too low to develop a practical process for NO removal. Isolation of the site and determination of the steps involved in the product formation may lead to development of an effective NO decomposition catalyst for removal of NO in an oxidizing environment.

5. Conclusion

Infrared spectroscopy coupled with mass spectroscopy allows determination of the form of NO_x storage during NO/O_2 adsorption and its behavior during TPDE/TPD. NO/O_2 coadsorbed as bridging and chelating bidentate nitrates and monodentate nitrate on Tb_4O_7, La_2O_3, and BaO, and as bridging bidentate nitrate and monodentate nitrate on MgO via the reaction of adsorbed NO with adsorbed oxygen at 298 K. NO/O_2 coadsorbed as a chelating bidentate nitrate on Tb_4O_7 and La_2O_3, and as a distinctive bridging bidentate nitrate on BaO and MgO via the reaction of adsorbed NO with surface lattice oxygen at 523 K.

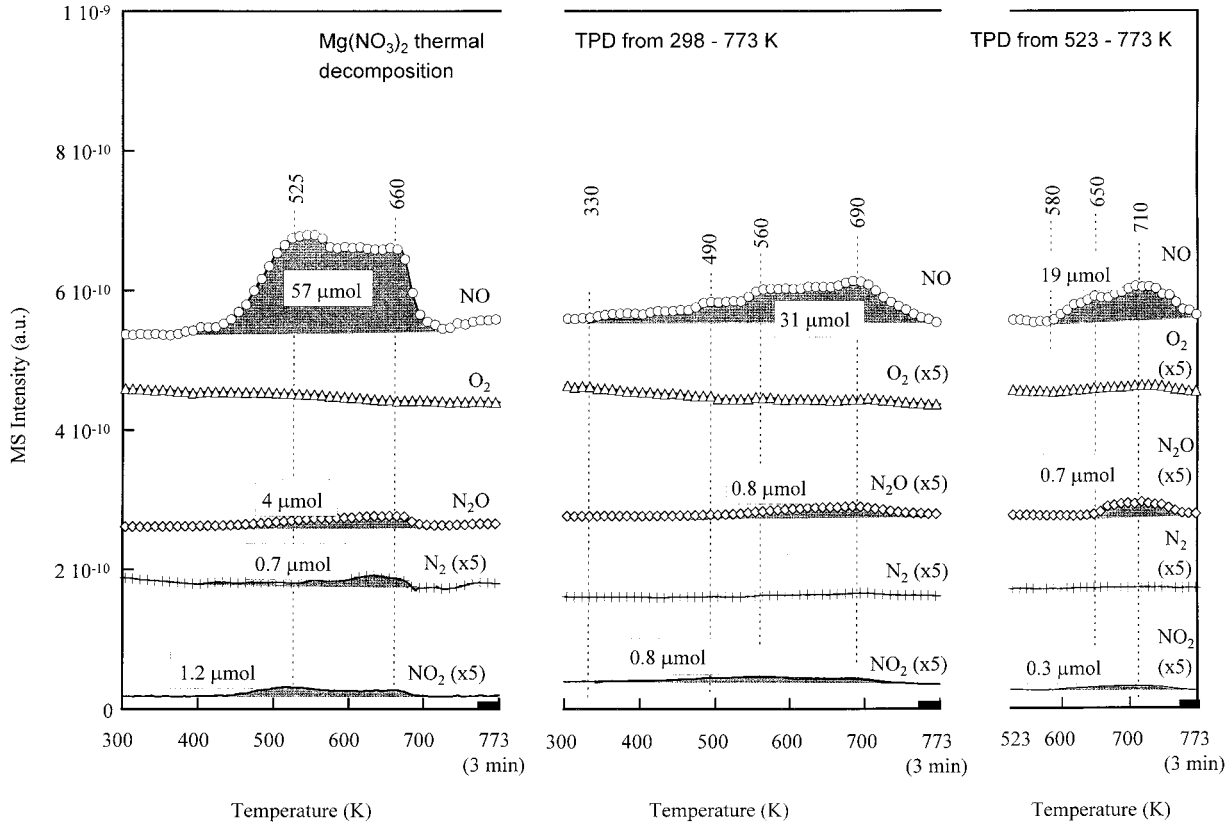

Figure 12. Normalized product MS profiles of (a) thermal decomposition of $Mg(NO_3)_2$ on γ-Al_2O_3, (b) TPD of adsorbates on MgO/γ-Al_2O_3 from 298 to 773 K, and (c) TPD of adsorbates on MgO/γ-Al_2O_3 from 523 to 773 K.

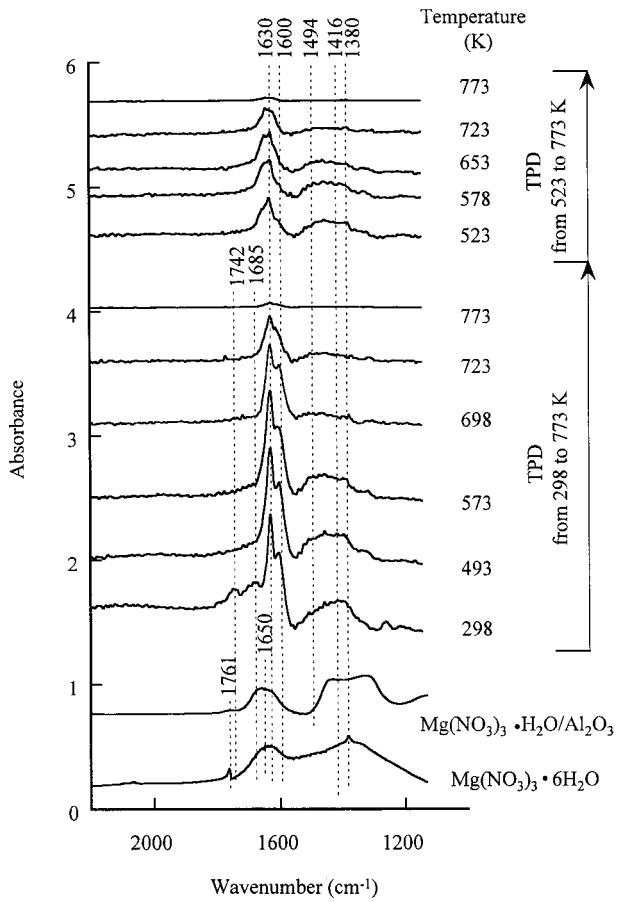

Figure 13. In situ IR spectra during TPD of adsorbates on MgO/γ-Al_2O_3 from 298/523 to 773 K as well as IR spectra of $Mg(NO_3)_2{\cdot}H_2O$/γ-Al_2O_3 and $Mg(NO_3)_2{\cdot}6H_2O$ at 298 K.

TPD of chelating bidentate nitrate on Tb_4O_7, La_2O_3, and BaO produced primarily NO and O_2, with maxima at 640 and 670 K, respectively. TPD of bridging bidentate nitrate and monodentate nitrate on Tb_4O_7, La_2O_3, and BaO produced NO and O_2 as major products and N_2 and N_2O as minor products at 320−500 K. Decomposition of bridging bidentate on MgO produced NO as a major product and N_2O as a minor product at a peak temperature of 690 K. Observation of NO and O_2 as major products of chelating and bridging bidentate nitrate decomposition suggests that the formation of these nitrates from NO and O_2 is essentially reversible without involvement of NO_2 as an intermediate. Peak temperatures for $Tb(NO_3)_3$, $La(NO_3)_3$, $Ba(NO_3)_2$, and $Mg(NO_3)_2$ decomposition occurred between those for bridging and chelating nitrates. The difference in reactivity and stability of chelating and bridging bidentate nitrates on various oxides may provide a wide range of operating temperatures for NO_x storage. Formation of N_2 from decomposition of various forms of nitrates suggests the need to identify the step involved in the conversion of nitrate to N_2. Identification of this step may guide the development of the oxide for conversion of NO in an oxidizing environment to N_2 and O_2 via metal nitrates.

Acknowledgment. The authors gratefully acknowledge the partial support of this research by the United States Department of Energy under Grant DE-FG22-95PC955224 and the Ohio Boards of Regents Research Challenge Grant. The assistance from Bei Chen and Pisanu Toochinda in performing these experiments is also appreciated.

References and Notes

(1) Taylor, K. C. *Catal. Rev.—Sci. Eng.* **1993**, *35*, 457.
(2) Masel, R. I. *Catal. Rev.—Sci. Eng.* **1986**, *28*, 335.

(3) Viswanathan, B. *Catal. Rev.—Sci. Eng.* **1992**, *34*, 337.
(4) Tabata, K.; Misono, M. *Catal. Today* **1990**, *8*, 249.
(5) Iwamoto, M. *Catal. Today* **1994**, *22*, 1.
(6) Shelef, M. *Catal. Rev.—Sci. Eng.* **1995**, *95*, 209.
(7) Yan, J. Y.; Satchtler, W. M. H.; Kung, H. H. *Catal. Today* **1997**, *33*, 279.
(8) Amiridis, M. D.; Zhuang, T.; Farrauto, R. J. *Appl. Catal., B* **1996**, *10*, 203.
(9) Li, Y.; Armor, L. *Appl. Catal.m B* **1995**, *5*, L257.
(10) Xie, S.; Mestl, G.; Rosynek, M. P.; Lunsford, J. H. *J. Am. Chem. Soc.* **1997**, *119*, 10186.
(11) Mestl, G.; Rosynek, M. P.; Lunsford, J. H. *J. Phys. Chem. B* **1997**, *101*, 9321.
(12) Mestl, G.; Rosynek, M. P.; Lunsford, J. H. *J. Phys. Chem. B* **1997**, *101*, 9329.
(13) Busca, G.; Lietti, L.; Ramis, G.; Berti, F. *Appl. Catal., B* **1998**, *18*, 1.
(14) Amiridis, M. D.; Duevel, R. V.; Waches, I. E. *Appl. Catal., B* **1999**, *20*, 111.
(15) Iwamoto, M.; Furukawa, H.; Mine, Y.; Uemura, F.; Mikuriya, S.; Kagawa, S. *J. Chem. Soc., Chem. Commun.* **1986**, *16*, 1272.
(16) Valyon, J.; Hall, W. K. *J. Phys. Chem.* **1993**, *97*, 1204.
(17) Aylor, A. W.; Larsen, S. C.; Reimer, J. A.; Bell, A. T. *J. Catal.* **1995**, *157*, 592.
(18) Li, Y.; Armor, J. N. *Appl. Catal., B* **1991**, *76*, L1.
(19) Curtin, T.; Delmon, B. *Catal. Today* **1997**, *35*, 121.
(20) Chuang, S. S. C.; Tan, C.-D. *J. Phys. Chem. B* **1997**, *101*, 3000.
(21) Machida, M.; Yasuoka, K.; Eguchi, K.; Arai, H. *J. Chem. Soc., Chem. Commun.* **1990**, *1*, 1165.
(22) Takahashi, N.; Shinjoh, H.; Iijima, T.; Suzuki, T.; Yamazaki, K.; Yokata, K.; Suzuki, H.; Miyoshi, N.; Matsumoto, S.; Tanizawa, T.; Tanaka, T.; Tateishi, S.; Kasahara, K. *Catal. Today* **1996**, *27*, 63.
(23) Eguchi, K.; Watabe, M.; Machida, M.; Arai, H. *Catal. Today* **1996**, *27*, 297.
(24) Mahzoul, H.; Brilhac, J. F.; Gilot, P. *Appl. Catal., B* **1999**, *20*, 47.
(25) Shimokawabe, M.; Tadokoro, K.; Sasaki, S.; Takezawa, N. *Appl. Catal., A* **1998**, *16*, 215.
(26) Bernal, S.; Blanco, G.; Cauqui, M. A.; Corchado, P.; Pintado, J. M.; Rodríguez-Izquierdo, J. M. *Chem. Commun.* **1997**, *16*, 1545.
(27) Klingenberg, B.; Vannice, M. A. *Appl. Catal., B* **1999**, *21*, 19.
(28) Zhang, X.; Walters, A. B.; Vannice, M. A. *J. Catal.* **1996**, *159*, 119.
(29) Munakata, F.; Akimune, Y.; Shichi, Y.; Yamaguchi, H.; Inoue, Y. *Chem. Commun.* **1997**, *1*, 63.
(30) Gordatos, H.; Gorte, R. J. *Appl. Catal., B* **1995**, *7*, 33.
(31) Fridell, E.; Skoglundh, M.; Westerberg, B.; Johansson, S.; Smedler, G. *J. Catal.* **1999**, *183*, 196.
(32) Acke, F.; Skoglundh, M. *J. Phys. Chem. B* **1999**, *103*, 972.
(33) Stark, J. V.; Klabunde, K. J. *Chem. Mater.* **1996**, *8*, 1913.
(34) Cerruti, L.; Modone, E.; Guglielminotti, E.; Borello, E. *J. Chem. Soc., Faraday Trans. 1* **1974**, *70*, 729.
(35) Chuang, S. S. C.; Brundage, M. A.; Balakos, M. W.; Srinivas, G. *Appl. Spectrosc.* **1995**, *49*, 1151.
(36) Vratny, F. *Appl. Spectrosc.* **1959**, *13*, 59.
(37) Addison, C. C.; Gatehouse, B. M. *J. Chem. Soc.* **1960**, 613.
(38) Ferraro, J. R. *J. Mol. Spectrosc.* **1960**, *4*, 99.
(39) Nyquist, R. A.; Kagel, R. O. *Infrared Spectra of Inorganic Compounds;* Academic Press: New York and London, 1971.
(40) Laane, J.; Ohlsen, J. R. *Prog. Inorg. Chem.* **1980**, *27*, 465.
(41) Outka, D. A.; Madix, R. J. *Surf. Sci.* **1987**, *179*, 1.
(42) Hadjiivanov, K.; Klissurski, D.; Ramis, G.; Busca, G. *Appl. Catal., B* **1996**, *7*, 251.
(43) Delahay, G.; Coq, B.; Ensuque, E.; Figuéras, F. *Langmuir* **1997**, *13*, 5588.
(44) Nakamoto, K. *Infrared and Raman Spectra of Inorganic and Coordination Compounds*, 4th ed.; Wiley: New York, 1986.
(45) Davynov, A. A. *Infrared Spectra of Adsorbed Species on the Surface of Transition Metal Oxides*; Rochester, C. H., Ed.; John Wiley & Sons: Chichester, England, 1990.
(46) Jenkins, R.; Snyder, R. L. *Introduction to X-ray Powder Diffractometry*; John Wiley & Sons: New York, 1996; Chapter 3.
(47) Xie, Y.-C.; Tang, Y.-Q. *Adv. Catal.* **1990**, *37*, 1.
(48) Ushakov, V. A.; Shkrabina, R. A.; Koryabkina, N. A.; Ismagilov, Z. R. *Kinet. Katal.* **1997**, *38*, 117.
(49) Groppi, G.; Cristiani, C.; Forzatti, P. *J. Mater. Sci.* **1994**, *29*, 3441.
(50) Ting, C.-J.; Lu, H.-Y. *J. Am. Ceram. Soc.* **1999**, *82*, 841.
(51) Béguin, B.; Garbowski, E.; Primet, M. *Appl. Catal.* **1991**, *75*, 119.
(52) Krim, L.; Lacome, N. *J. Phys. Chem. B* **1998**, *102*, 2289.
(53) Terenin, A.; Reov, L. *Spectrochim. Acta* **1959**, *11*, 946.
(54) Xu, X.; Chen, P.; Goodman, D. W. *J. Phys. Chem. B* **1994**, *98*, 9242.
(55) Hoost, T. E.; Otto, K.; Laframboise, K. A. *J. Catal.* **1995**, *155*, 303.
(56) Almusaiteer, K.; Chuang, S. S. C. *J. Catal.* **1998**, *180*, 161.
(57) Henrich, V. E.; Cox, P. A. *Appl. Surf. Sci.* **1993**, *72*, 277.
(58) Martínez-Arias, A.; Soria, J.; Conesa, J. C.; Seoane, X. L.; Arcoya, A.; Cataluña, R. *J. Chem. Soc., Faraday Trans. 1* **1995**, *91*, 1679.
(59) Yanagisawa, Y. *Appl. Surf. Sci.* **1995**, *89*, 251.
(60) Forni, L.; Oliva, C.; Barzetti, T.; Selli, E.; Ezerets, A. M.; Vishniakov, A. V. *Appl. Catal., B* **1997**, *13*, 35.
(61) Che, M.; Tench, A. J. *Adv. Catal.* **1983**, *32*, 1.
(62) Bielański, A.; Haber, J. *Oxygen in Catalysis;* Marcel Dekker:New York, 1991.
(63) Borchert, H.; Baerns, M. *J. Catal.* **1997**, *168*, 315.
(64) Lunsford, J. H. *Catal. Rev.* **1973**, *8*, 135.
(65) Iwamoto, M.; Yoda, Y.; Yamazoe, N.; Seiyama, T. *J. Phys. Chem.* **1978**, *82*, 2564.
(66) Al-Mashta, F.; Sheppard, N.; Lorenzell, V.; Busca, G. *J. Chem. Soc., Faraday Trans. 1* **1982**, *78*, 979.
(67) Kung, H. H. *Stud. Surf. Sci. Catal.* **1989**, *45*, 1.
(68) Henrich, V. E.; Cox, P. A. *The Surface Science of Metal Oxides;* Cambridge University Press: 1994.
(69) Holmgren, A.; Duprez, D.; Andersson, B. *J. Catal.* **1999**, *182*, 441.
(70) Balasubramanian, S. Master's thesis, The University of Akron, 1998, p 64.
(71) Schraml-Marth, M.; Wokaun, A.; Baiker, A. *J. Catal.* **1992**, *138*, 306.
(72) Gates, B. C. *Catalytic Chemistry;* John Wiley & Sons:1992.
(73) Chi, Y.; Chuang, S. S. C. *J. Catal.* **2000**, *190*, 75.
(74) Perry, D. L.; Philipps, S. L. *Handbook of Inorganic Compounds;* CRC Press: Boca Raton, FL, 1995; p 54.
(75) Chi, Y.; Chuang, S. S. C. Unpublished work.
(76) Ettarh, C.; Galwey, A. K. *Thermochim. Acta* **1996**, *288*, 203.